ISSN 0015-4628, Fluid Dynamics, 2017, Vol. 52, No. 4, pp. 468–480. © Pleiades Publishing, Ltd., 2017.
Original Russian Text © A.G. Bagoutdinova, E.K. Vachagina, Ya.D. Zolotonosov, 2017, published in Izvestiya Rossiiskoi Akademii Nauk, Mekhanika Zhidkosti i Gaza, 2017, No. 4, pp. 9–23.

Viscous Laminar Flow in Smooth Coil Tubes

A. G. Bagoutdinova[a*], E. K. Vachagina[b], and Ya. D. Zolotonosov[a***]**

[a]*Kazan State University of Architecture and Engineering, ul. Zelenaya 1, Kazan, 420043 Russia*

[b]*Kazan Scientific Center of Russian Academy of Sciences, ul. Lobachevskogo 2/31, Kazan, 420111 Russia*

*e-mail: *bagoutdinova@rambler.ru, **vachaginae@mail.ru, ***zolotonosov@mail.ru*

Received July 1, 2016

Abstract—A mathematical model of incompressible viscous laminar flow in smooth coil tubes is proposed and the results of its numerical realization in a nonorthogonal helical coordinate system are presented. This coordinate system is free of singularities in the domain of definition of the unknown functions, that is, the pressure and the velocity components, which makes it possible to refine the existing distributions of the axial component and the secondary crossflows obtained using the well-known orthogonal coordinate system having a singularity at the center of the coil channel. The momentum transport equation is written in the projections on the axes of the natural basis of the coordinate system, which makes it possible to subdivide the system of equations into two alternately solved subsystems. The distributions of the axial and two transverse components show that at the center of coil tubes the transverse components are comparable with the axial velocity (the transverse components can be as high as half the mean-flow-rate velocity and one third of it at the center of the channel).

Keywords: heat transfer, fluid dynamics, mathematical models, helix, coil tubes, helical coordinate system, metric tensor.

DOI: 10.1134/S0015462817040020

Curved coil tubes are conventionally used as effective component parts of the present-day heat-exchange equipment [1–11].

Widely used in the industry are the coil tubes [1–4, 12–15] with a constant radius of the helical spiral bend immersed in a reservoir with a fluid. The methods of their engineering calculation are described in both the Russian [16] and foreign [12–15, 17–19] literature. In this connection, the detailed theoretical and experimental investigations of the hydrodynamic and heat-transfer processes in the flow-through sections of curved coil tubes seem very topical.

The foundation for developing the mathematical models of viscous flows is given by studies [20–23], where flows in the channels with a slightly curved axis were investigated. These flows were described using the simplified Navier–Stokes equations for curved tubes with a small curvature of the axis. Later, this approach was applied in the case of laminar fluid flows in coils [24, 25].

Typical of laminar flows in coil tubes with arbitrary values of the curvature and the torsion of the central helical line are, as in flows in turns (toruses), secondary flows [7]. Precisely the transverse circulation of the fluid in flow-through sections of the curvilinear channels under consideration is the main reason for the enhancement of heat-transfer processes [5–10]. Natural for these flows are the suppositions on the importance of the secondary flows at the center of a coil tube and of a nonsymmetric distribution of the transverse velocity components in a section relative to the line whose direction vector coincides with the vector of the principal normal to the central helical line. Thus, the transverse components in the orthogonal coordinate system cannot be determined at the center of a section [24, 25]; they considerably vary in its vicinity and can be assessed only with large errors. In this case, different simplifications and approximations

are invoked, which, however, do not allow one to estimate in the full measure the velocity fields in the central region of a channel [26]. The use of the nonorthogonal coordinate system proposed below makes it possible to obtain a more accurate flowfield pattern in this region.

There are known some studies, for example, [12, 19], that use numerical methods for solving the problems of viscous flow in coils written in the Cartesian coordinate system in the three-dimensional formulation. In this case, the helical symmetry is not taken into account and the necessary amount of numerical calculations becomes unwarrentedly large. Well-known in the literature and fairly completely described are also special helical coordinate systems [24, 25, 27–30], which make it possible to reduce the solution of three-dimensional problems to two-dimensional ones. In [24, 25] orthogonal and nonorthogonal coordinate systems were proposed. However, the orthogonal system has one shortcoming, namely, the translation along the helix is not the translation along one of the independent variables. Because of this, after the system of governing equations has been written in the orthogonal system, the inverse passage to the variables of the nonorthogonal system is inevitable.

The fractional step method proposed in [31] for analyzing the heat transfer processes in laminar flows with fully formed velocity and pressure profiles in curved toroidal tubes uses the toroidal coordinate system. In this case, the solution of the problem formulated depends only on two variables determined in the cross-section of the curved tube. In view of the fact that at the center of the cross-section of a toroidal tube there is the singular point of this coordinate system (the Jacobian is zero), in [31] it was proposed to use the symmetry of the flows under consideration about the line passing through the vector of the principal normal to the axial line of tube and to seek the unknown velocity and pressure fields only in one half of the cross-section. This approach makes it possible to pass over the singular point of the system. In our case, in which the axial line torsion must be taken into account, the symmetry condition is violated and the consideration of the flow only in a half of the cross-section becomes unjustified. However, the approach [31] can be used in the case of flow in coil tube, when the bend radius is considerable greater than the diameter of its flow-through section [32–34].

As shown in [7], the heat transfer effect is considerably greater in the coil heat-exchangers with a small bend radius of the coil, since the effect of toroidal vortex formation and mixing most clearly manifests itself in the flow-through sections of these tubes. The special feature of these flows is that they are different from the hydrodynamic conditions of flows in toroidal tubes, earlier comprehensively considered in [31]. Owing to the violation of the flow symmetry in the tubes, a flow analysis in only half of the cross-section becomes inadequate.

The main purpose of this study is to obtain and to analyze the hydrodynamic characteristics over wide ranges of the geometric and regime parameters throughout the entire flow region, including the central regions of the coil tubes under consideration. Since the crossflows are the reason for an enhancement of heat-transfer processes in the coil tubes, it is necessary to obtain the profiles of the transverse velocity components in order to estimate their values, compared with the axial flows.

1. MATHEMATICAL MODEL

Since the geometric shape of the coil channels and the system of equations of motion and continuity are invariant with respect to translations along the helical spiral, we note the fact of the existence and uniqueness of the solution of this system under certain restrictions imposed on the Reynolds number [35]. When using the conventional Cartesian coordinate system the numerical solution essentially depends on three spatial coordinates, which makes the calculations considerably more difficult and diminishes their accuracy and the processing and presentation of the results obtained.

We will assume that the incompressible fluid flow is steady, isothermal, and laminar. In the fluid flows in coil channels the density ρ varies only slightly.

For the purpose of using the geometric symmetry of the coil channels we will consider the helical coordinate system related with the Cartesian coordinate system by the following equations

$$x = \frac{d}{2}\kappa\cos\xi^3 + \frac{d}{2}\left(-\xi^1\cos\xi^3 + \xi^2\frac{w\sin\xi^3}{\sqrt{1+w^2}}\right),$$
$$y = \frac{d}{2}\kappa\sin\xi^3 + \frac{d}{2}\left(-\xi^1\sin\xi^3 - \xi^2\frac{w\cos\xi^3}{\sqrt{1+w^2}}\right), \tag{1.1}$$
$$z = \frac{d}{2}\kappa w\xi^3 + \frac{d}{2}\frac{\xi^2}{\sqrt{1+w^2}},$$

where $\kappa = 2R/d$ and $w = S/(2\pi R)$ are the parameters of the central helix, S is the helical channel pitch, $d/2$ is the coil tube radius, and R is the bend radius of the central helical line of the coil tube.

Any curve is usually characterized by two parameters, namely, the curvature k and the torsion τ [24, 25, 29]. In particular, for a helical line we can write

$$k = \frac{R}{R^2 + (S/(2\pi))^2}, \qquad \tau = \frac{S/(2\pi)}{R^2 + (S/(2\pi))^2}.$$

It might be expected that the problem solution depends on the curvature, the torsion, and the Reynolds number. As shown in [25], for the helical axial line the problem solution depends on the ratio $\lambda = \tau/k = S/(2\pi R) = w$ and the Reynolds number. In our case, the solution is determined by two geometric simplexes, κ and $\sigma = w/\sqrt{1+w^2}$. The parameter σ is a function of λ, while the parameter κ is responsible for the ratio of the bend radius of the central helix to the coil tube radius.

For the adequacy of the passage from the Cartesian to the helical coordinate system it is necessary to ensure the condition that the corresponding Jacobian of the passage is nonzero

$$J = \left(\frac{d}{2}\right)^2 \frac{1}{\sqrt{1+w^2}}(\kappa(1+w^2) - \xi^1) \neq 0.$$

Hence it follows that the one-to-one correspondence between the Cartesian x, y, z and helical ξ^1, ξ^2, ξ^3 coordinates is valid at $\xi^1 \neq \kappa(1+w^2)$ or $\kappa(1+w^2) > 1$. This condition is always fulfilled, since $\kappa > 1$.

In [30] the similar problem was solved in the coordinate system, whose parameters depended on the curvature and the torsion. The Navier–Stokes equations were written in the projections on two vectors of the natural basis and on one vector of the dual basis directed perpendicular to the plane of the two former vectors. As a result, the unknown function of the dimensionless pressure was present in three equations, which made the calculations considerably more difficult and diminished their accuracy.

In our case, the ξ^1, ξ^2, ξ^3 coordinate system has the following characteristics.

The covariant components of the metric tensor divided by $(d/2)^2$ take the form:

$$g_{11} = 1, \quad g_{22} = 1, \quad g_{33} = \left((\xi^1 - \kappa)^2 + \sigma^2(\xi^2)^2 + w^2\kappa^2\right),$$
$$g_{12} = g_{21} = 0, \quad g_{13} = g_{31} = -\sigma\xi^2, \quad g_{23} = g_{32} = \sigma\xi^1.$$

The contravariant components of the metric tensor divided by $1/(d/2)^2$ are as follows:

$$g^{11} = \frac{((1+w^2)\kappa - \xi^1)^2 + w^2(\xi^2)^2}{((1+w^2)\kappa - \xi^1)^2}, \qquad g^{22} = \frac{((1+w^2)\kappa - \xi^1)^2 + w^2(\xi^1)^2}{((1+w^2)\kappa - \xi^1)^2},$$
$$g^{33} = \frac{(1+w^2)}{((1+w^2)\kappa - \xi^1)^2}, \qquad g^{12} = g^{21} = -\frac{w^2\xi^1\xi^2}{((1+w^2)\kappa - \xi^1)^2},$$
$$g^{13} = g^{31} = \frac{w\sqrt{1+w^2}\xi^2}{((1+w^2)\kappa - \xi^1)^2}, \qquad g^{23} = g^{32} = -\frac{w\sqrt{1+w^2}\xi^1}{((1+w^2)\kappa - \xi^1)^2}.$$

The nonzero Cristoffel symbols of the first kind normalized by $d/2$ are as follows:

$$\Gamma_{31,2} = \Gamma_{13,2} = \sigma, \quad \Gamma_{32,1} = \Gamma_{23,1} = -\sigma, \quad \Gamma_{32,3} = \Gamma_{23,3} = \sigma^2\xi^2, \quad \Gamma_{33,2} = -\sigma^2\xi^2,$$
$$\Gamma_{31,3} = \Gamma_{13,3} = (\xi^1 - \kappa), \qquad \Gamma_{33,1} = -(\xi^1 - \kappa).$$

Those of the second kind are as follows:

$$\Gamma^1_{33} = g^{11}\Gamma_{33,1} + g^{12}\Gamma_{33,2}, \quad \Gamma^2_{33} = g^{21}\Gamma_{33,1} + g^{22}\Gamma_{33,2}, \quad \Gamma^3_{33} = g^{31}\Gamma_{33,1} + g^{32}\Gamma_{33,2},$$
$$\Gamma^1_{31} = \Gamma^1_{13} = g^{12}\Gamma_{13,2} + g^{13}\Gamma_{13,3}, \qquad \Gamma^2_{31} = \Gamma^2_{13} = g^{22}\Gamma_{13,2} + g^{23}\Gamma_{13,3},$$
$$\Gamma^3_{31} = \Gamma^3_{13} = g^{32}\Gamma_{13,2} + g^{33}\Gamma_{13,3}, \qquad \Gamma^1_{32} = \Gamma^1_{23} = g^{11}\Gamma_{23,1} + g^{13}\Gamma_{23,3}.$$

Clearly that, as distinct from the orthogonal coordinate system of general form, the following Cristoffel symbols are additionally nonzero. These are two symbols of the fist kind, $\Gamma_{31,2} = \Gamma_{13,2} = \sigma$ and $\Gamma_{32,1} = \Gamma_{23,1} = -\sigma$ and two symbols of the second kind, $\Gamma^2_{31} = \Gamma^2_{13} = g^{22}\Gamma_{13,2} + g^{23}\Gamma_{13,3}$ and $\Gamma^1_{32} = \Gamma^1_{23} = g^{11}\Gamma_{23,1} + g^{13}\Gamma_{23,3}$.

In the chosen coordinate system (1.1) and in the projections on the natural axes the system of equations of motion and continuity takes the form:

$$\mathrm{Re}_*\Big(g_{11}V^1\frac{\partial V^1}{\partial\xi^1} + g_{11}V^2\frac{\partial V^1}{\partial\xi^2} + g_{13}V^1\frac{\partial V^3}{\partial\xi^1} + g_{13}V^2\frac{\partial V^3}{\partial\xi^2}$$
$$+2(g_{11}\Gamma^1_{13} + g_{13}\Gamma^3_{13})V^1V^3 + 2g_{11}\Gamma^1_{23}V^2V^3 + (g_{11}\Gamma^1_{33} + g_{13}\Gamma^3_{33})V^3V^3) \tag{1.2}$$
$$= -\frac{\partial p}{\partial\xi^1} + \Big(\frac{\partial B^1_1}{\partial\xi^1} + \frac{\partial B^1_1}{\partial\xi^2} - \Gamma^1_{13}B^3_1 - \Gamma^2_{13}B^3_2 - \Gamma^3_{13}B^3_3 + \Gamma^3_{31}B^1_1\Big),$$

$$\mathrm{Re}_*\Big(g_{22}V^1\frac{\partial V^2}{\partial\xi^1} + g_{22}V^2\frac{\partial V^2}{\partial\xi^2} + g_{23}V^1\frac{\partial V^3}{\partial\xi^1} + g_{23}V^2\frac{\partial V^3}{\partial\xi^2}$$
$$+2(g_{22}\Gamma^2_{13} + g_{23}\Gamma^3_{13})V^1V^3 + (g_{22}\Gamma^2_{33} + g_{23}\Gamma^3_{33})V^3V^3) \tag{1.3}$$
$$= -\frac{\partial p}{\partial\xi^2} + \Big(\frac{\partial B^1_2}{\partial\xi^1} + \frac{\partial B^2_2}{\partial\xi^2} - \Gamma^1_{23}B^3_1 + \Gamma^3_{31}B^1_2\Big),$$

$$\mathrm{Re}_*\Big(g_{31}V^1\frac{\partial V^1}{\partial\xi^1} + g_{31}V^2\frac{\partial V^1}{\partial\xi^2} + g_{32}V^1\frac{\partial V^2}{\partial\xi^1} + g_{32}V^2\frac{\partial V^2}{\partial\xi^2} + g_{33}V^1\frac{\partial V^3}{\partial\xi^1} + g_{33}V^2\frac{\partial V^3}{\partial\xi^2}$$
$$+2(g_{31}\Gamma^1_{13} + g_{32}\Gamma^2_{13} + g_{33}\Gamma^3_{13})V^1V^3 + 2g_{31}\Gamma^1_{23}V^2V^3 + (g_{31}\Gamma^1_{33} + g_{32}\Gamma^2_{33} + g_{33}\Gamma^3_{33})V^3V^3) \tag{1.4}$$
$$= -\frac{\partial p}{\partial\xi^3} + \Big(\frac{\partial B^1_3}{\partial\xi^1} + \frac{\partial B^2_3}{\partial\xi^2} - \Gamma^1_{31}B^1_1 - \Gamma^1_{32}B^2_1 - \Gamma^1_{33}B^3_1 - \Gamma^2_{31}B^1_2 - \Gamma^2_{33}B^3_2 - \Gamma^3_{33}B^3_3\Big),$$

$$\frac{\partial V^1}{\partial\xi^1} + \frac{\partial V^2}{\partial\xi^2} + \Gamma^3_{31}V^3 = 0, \tag{1.5}$$

where $\mathrm{Re}_* = V_a d\rho/(2\mu)$ is the modified Reynolds number, $p = dP/(2\mu V_a)$ is the dimensionless pressure, V_a is the characteristic velocity, ρ is the density, and μ is the dynamic viscosity.

The dimensionless components of the White–Metzner tensor $B = 2D$ take the form:

$$B^{11} = 2g^{11}\Big(\frac{\partial V^1}{\partial\xi^1}\Big) + 2g^{12}\Big(\frac{\partial V^1}{\partial\xi^2}\Big) + 2g^{13}\Gamma^1_{13}V^1 + 2g^{13}\Gamma^1_{23}V^2,$$
$$B^{22} = 2g^{21}\Big(\frac{\partial V^2}{\partial\xi^1}\Big) + 2g^{22}\Big(\frac{\partial V^2}{\partial\xi^2}\Big) + 2g^{23}\Gamma^2_{13}V^1,$$
$$B^{33} = 2g^{31}\Big(\frac{\partial V^3}{\partial\xi^1}\Big) + 2g^{32}\Big(\frac{\partial V^3}{\partial\xi^2}\Big) + 2g^{33}\Gamma^3_{13}V^1,$$
$$B^{12} = g^{11}\Big(\frac{\partial V^2}{\partial\xi^1}\Big) + g^{22}\Big(\frac{\partial V^1}{\partial\xi^2}\Big) + (g^{23}\Gamma^1_{13} + g^{13}\Gamma^2_{13} - g^{21}\Gamma^3_{31})V^1 + g^{23}\Gamma^1_{23}V^2,$$
$$B^{13} = g^{31}\Big(\frac{\partial V^1}{\partial\xi^1}\Big) + g^{32}\Big(\frac{\partial V^1}{\partial\xi^2}\Big) + g^{11}\Big(\frac{\partial V^3}{\partial\xi^1}\Big) + g^{12}\Big(\frac{\partial V^3}{\partial\xi^2}\Big) + (g^{33}\Gamma^1_{13} + g^{13}\Gamma^3_{13})V^1 + g^{33}\Gamma^1_{23}V^2,$$
$$B^{23} = g^{31}\Big(\frac{\partial V^2}{\partial\xi^1}\Big) + g^{32}\Big(\frac{\partial V^2}{\partial\xi^2}\Big) + g^{21}\Big(\frac{\partial V^3}{\partial\xi^1}\Big) + g^{22}\Big(\frac{\partial V^3}{\partial\xi^2}\Big) + (g^{33}\Gamma^2_{13} + g^{23}\Gamma^3_{13})V^1,$$

$$B_1^1 = g_{1k}B^{k1} = g_{11}B^{11} + g_{13}B^{31} = B^{11} - \sigma\xi^2 B^{31},$$
$$B_1^2 = g_{1k}B^{k2} = g_{11}B^{12} + g_{13}B^{32} = B^{12} - \sigma\xi^2 B^{32},$$
$$B_1^3 = g_{1k}B^{k3} = g_{11}B^{13} + g_{13}B^{33} = B^{13} - \sigma\xi^2 B^{33},$$
$$B_2^1 = g_{2k}B^{k1} = g_{22}B^{21} + g_{23}B^{31} = B^{21} + \sigma\xi^1 B^{31},$$
$$B_2^2 = g_{2k}B^{k2} = g_{22}B^{22} + g_{23}B^{32} = B^{22} + \sigma\xi^1 B^{32},$$
$$B_2^3 = g_{2k}B^{k3} = g_{22}B^{23} + g_{23}B^{33} = B^{23} + \sigma\xi^1 B^{33},$$
$$B_3^1 = g_{3k}B^{k1} = g_{31}B^{11} + g_{32}B^{21} + g_{33}B^{31} = -\sigma\xi^2 B^{11} + \sigma\xi^1 B^{21} + \phi B^{31},$$
$$B_3^2 = g_{3k}B^{k2} = g_{31}B^{12} + g_{32}B^{22} + g_{33}B^{32} = -\sigma\xi^2 B^{12} + \sigma\xi^1 B^{22} + \phi B^{32},$$
$$B_3^3 = g_{3k}B^{k3} = g_{31}B^{13} + g_{32}B^{23} + g_{33}B^{33} = -\sigma\xi^2 B^{13} + \sigma\xi^1 B^{23} + \phi B^{33},$$

where $\phi = ((\xi^1 - \kappa)^2 + \sigma^2(\xi^2)^2 + w^2\kappa^2)$ and $D = 1/2(\operatorname{grad}\mathbf{V} + \operatorname{grad}\mathbf{V}^T)$ is the strain rate tensor.

The geometric domain, where the system of equations (1.2)–(1.5) is fulfilled, is the cross-section of the coil tube, namely, the circle of unit radius in the plane of the variables ξ^1, ξ^2.

The system of equation written above must be supplemented with the uniqueness conditions, namely, the given value of the fluid flow rate Q through the channel cross-section and the no-slip conditions imposed on the inner channel wall.

Equations (1.2)–(1.5) are written in the projections on the natural coordinate axes, where the contravariant velocity components are used, while the term including $\operatorname{div}(\mu B)$ is not transformed to the form $\mu \operatorname{grad}\mathbf{V}$ or $\mu \operatorname{curl}\operatorname{curl}\mathbf{V}$, which makes it possible to use in what follows the system of hydrodynamic equations obtained in the case, in which the fluid viscosity is a function of either the temperature or the second invariant of the strain rate tensor. In the case of isothermal flows the tensor of the velocity gradient $\operatorname{grad}\mathbf{V}$ can be used instead of the White–Metzner tensor. For the sake of comparison we made the calculations in which $\operatorname{grad}\mathbf{V}$ is used, as the tensor B. The error of the calculations is in this case not greater than 1%.

To investigate the solutions of system (1.2)–(1.5) it is necessary to pass to dimensionless variables, which makes it possible to postulate the dependence of the solution on three complexes, namely, the Reynolds number and two geometric simplexes κ and w. The former geometric simplex describes the dependence of the solution on the channel curvature and the latter represents the dependence on the helix pitch.

In the general case of laminar flows the problem solution depends on three parameters: Re, κ, and w.

The system of equations (1.2)–(1.5), subject to the uniqueness conditions, was solved using the finite element method.

Since the main variables in the equations of motion are the dimensionless contravariant velocity components V^1, V^2, and V^3, the passage to the dimensionless contravariant components was made according to the formulas

$$V_1 = V^1 - \sigma\xi^2 V^3, \qquad V_2 = V^2 + \sigma\xi^1 V^3,$$
$$V_3 = -\sigma\xi^2 V^1 + \sigma\xi^1 V^2 + ((\xi^1 - \kappa)^2 + \sigma w(\xi^2)^2 + w^2\kappa^2)V^3.$$

In the general case of spiral channels different velocity components and their projections on different axis directions can be employed. In analyzing the results of the numerical calculations it is convenient to subdivide the velocity vector into two parts, $\mathbf{V} = \mathbf{U} + \mathbf{W}$, where $\mathbf{U} = \mathbf{V} - (V^3/g^{33})\mathbf{e}^3 = (V_1/g_{11})\mathbf{e}_1 + (V_2/g_{22})\mathbf{e}_2$ is the vector in the plane perpendicular to the central helical line, and $\mathbf{W} = (V^3/g^{33})\mathbf{e}^3$ is the vector tangent to the central helical line $\mathbf{U}$ and perpendicular to the cross-sectional plane. Here, $\mathbf{e}_1$, $\mathbf{e}_2$, and $\mathbf{e}_3$ are the vectors of the natural basis defined as $\mathbf{e}_i = \partial\mathbf{r}/\partial\xi^i$, where $\mathbf{r}$ is the radius-vector of an arbitrary point in space, and $\mathbf{e}^1$, $\mathbf{e}^2$, and $\mathbf{e}^3$ are the vectors of the dual basis. While the system of the vectors $\mathbf{e}_1$, $\mathbf{e}_2$, $\mathbf{e}_3$ is orthogonal, the system of coordinates ξ^1, ξ^2, ξ^3 is not orthogonal, since the orthogonal system is considered to mean such a system in which the covariant $g_{ij} = (\mathbf{e}_i \cdot \mathbf{e}_j)$ and the contravariant $g^{ij} = (\mathbf{e}^i \cdot \mathbf{e}^j)$ components of the metric tensor form a diagonal matrix.

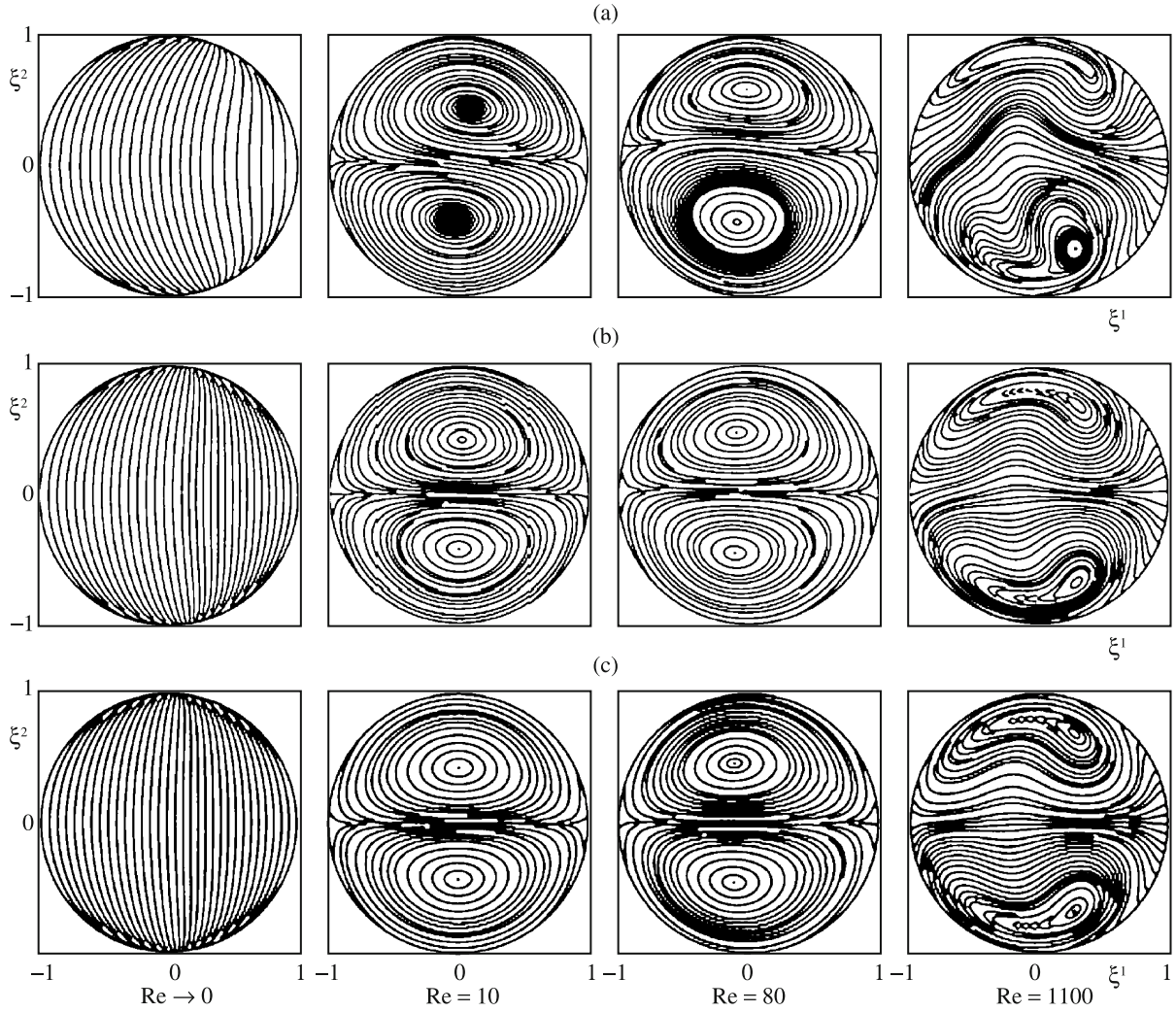

Fig. 1. Streamlines of crossflows in laminar flows in the coils with the relative pitch $S/D = 1.5$ for different Reynolds numbers; (a–c) relate to $R/d = 1$, 2.5, and 5.

2. RESULTS OF THE NUMERICAL CALCULATIONS

Figures 1 to 7 present the results of a numerical investigation of viscous flows in curved coil tubes. The Reynolds number was taken to be Re = 0, 10, 80, and 1100, the dimensionless radius of curvature varied on the range $1 < R/d < 5$, and the value of the relative coil pitch $S/d = 1.5$ taken in the calculations is that most frequently encountered in practice.

In Fig. 1 we have plotted the streamlines of the crossflows, that is, the lines, whose tangents coincide with the direction of the velocity vector **U** component lying in the cross-section. As follows from the calculations (Re $\to$ 0), the "streamlines" of the transverse velocity component are directed parallel to the vector $\mathbf{e}_2$. The absolute values of the transverse velocities $V_1/\sqrt{g_{11}}$ and $V_2/\sqrt{g_{22}}$ (Fig. 3) can be considered as negligibly small (by a factor of 100 and more smaller than the third component $V^3/\sqrt{g^{13}}$ in Fig. 7). With increase in the Reynolds number (Re = 10 to 100) the velocity field restructures itself: the streamlines in the upper left and lower right wall regions form pairwise vortices which then grow in dimensions. When the value of the central helix curvature is fairly large, $R/d = 1$, the dimensions of the upper vortex region are considerably smaller than those of the lower region. With further increase in the Reynolds number (Re = 100 to 1000) the coil tube flow changes in nature, which is reflected on the streamline deformation pattern and the displacement of the vortex formation centers toward the peripheral tube walls. In the coils with the parameters $R/d = 2.5$ and 5 the fluid flow becomes similar with that in toroidal tubes, while the

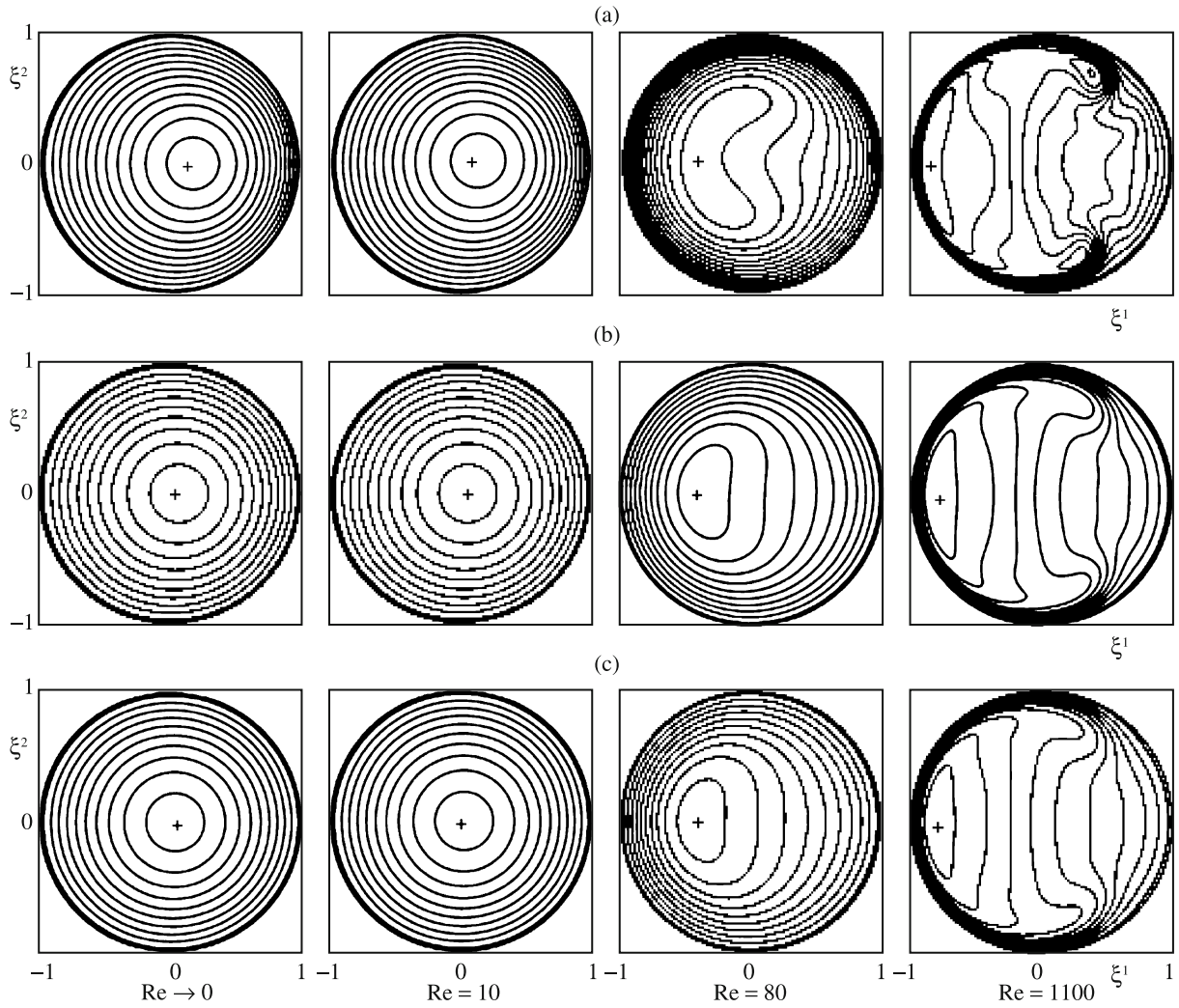

Fig. 2. Contours of the dimensionless contravariant velocity component $V^3/\sqrt{g^{33}}$ directed perpendicular to the cross-section with the relative pitch $S/d = 2.5$ for different Re. The regions of the positive and negative values of the presented quantity are labelled by the plus and minus signs, The other notation same as in Fig. 1.

vortex regions become symmetric about the horizontal axis ξ^1. With increase in the parameter R/d the process of pairwise vortex formation is completed at smaller Reynolds numbers, the transverse circulatory velocity component becomes negligibly small, and the fluid flow becomes similar with that in a rectilinear round tube. The qualitative pattern of the transverse circulation streamlines coincides with the data of studies [24, 25, 30].

In Fig. 2 we have plotted the contours of the dimensionless contravariant velocity component $V^3/\sqrt{g^{33}}$ which takes only positive values. This component has a unique maximum, which in slow motions (in the Stokes approximation, as $\mathrm{Re} \to 0$) is displaced rightward, toward the center of curvature of the helical line, which especially clearly manifests itself in the case in which $R/d = 1$. With increase in the Reynolds number ($\mathrm{Re} = 10$ to 80) and the centrifugal force this maximum is displaced leftward. At the same time, with increase in Re the tube flow pattern alters and the contours, which had earlier the shape of circles, are deformed and extended along the vertical axis. The flow development ($\mathrm{Re} = 80$ to 1000) results in the further deformation of the contours, while the fluid is pushed toward the left boundary of the tube cross-section with the formation of two additional local maxima in the upper and lower wall regions. In the coil with $R/d = 1$ the distribution of the contravariant component $V^3/\sqrt{g^{33}}$ is asymmetric: under the influence of the channel wall the contours rotate clockwise. With increase in R/d to 2.5 and 5 and as $\mathrm{Re} \to 0$ the

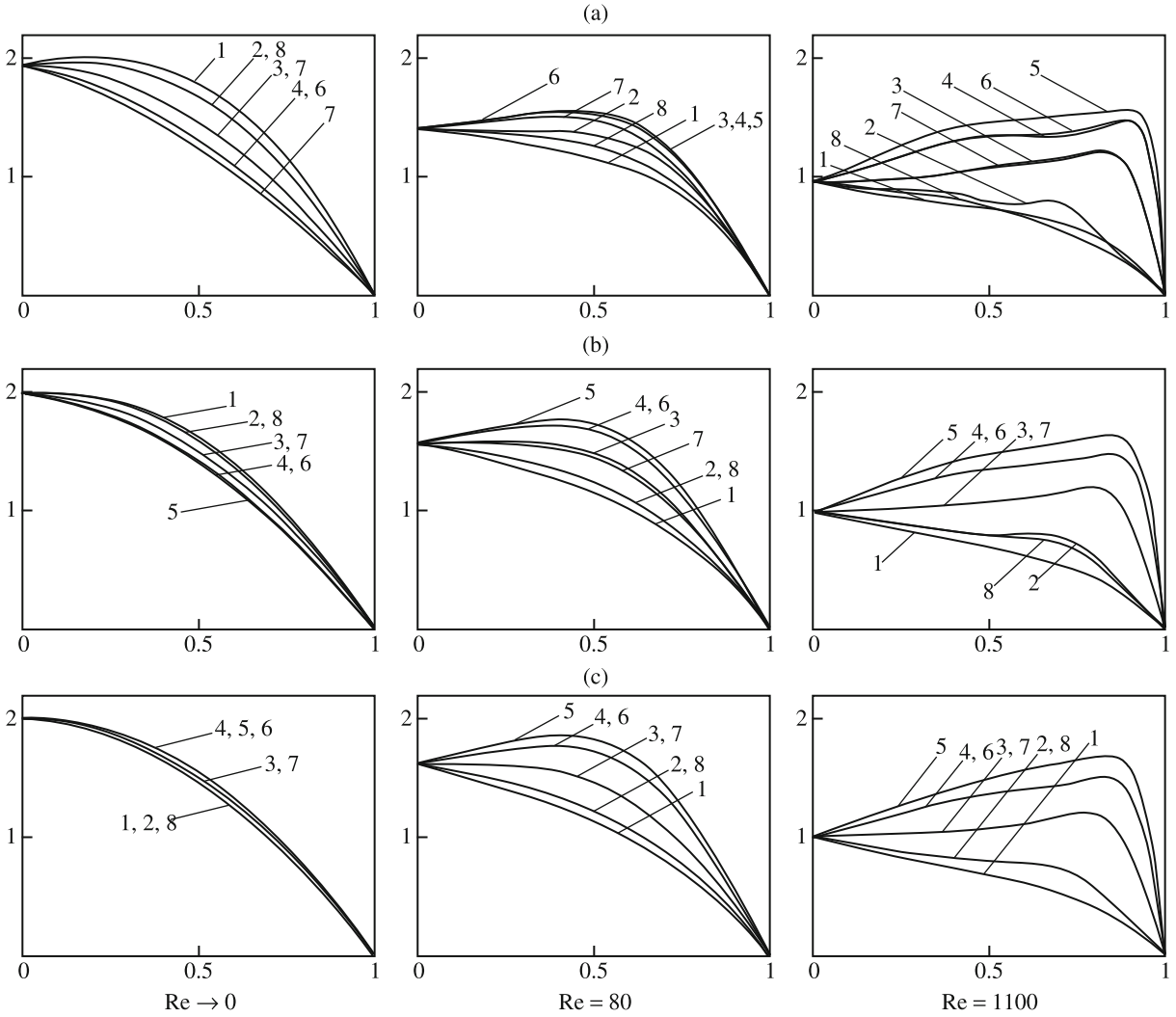

Fig. 3. Profiles of the covariant physical component $V_3/\sqrt{g_{33}}$ of the velocity vector for different Re with the relative pitch $S/d = 2.5$ along the lines (*1*) $\xi^2 = 0$, $0 \le \xi^1 \le 1$; (*2*) $\xi^2 = \xi^1$, $0 \le \xi^1 \le \sqrt{2}/2$; (*3*) $\xi^1 = 0$, $0 \le \xi^2 \le 1$; (*4*) $\xi^2 = -\xi^1$, $-\sqrt{2}/2 \le \xi^1 \le 0$; (*5*) $\xi^2 = 0$, $-1 \le \xi^1 \le 0$; (*6*) $\xi^2 = \xi^1$, $-\sqrt{2}/2 \le \xi^1 \le 0$; (*7*) $\xi^1 = 0$, $-1 \le \xi^2 \le 0$; and (*8*) $\xi^2 = -\xi^1$, $0 \le \xi^1 \le \sqrt{2}/2$. The other notation same as in Fig. 1.

maximum displacement becomes less noticeable, while the distribution of the level lines approaches the symmetrical distribution about the horizontal axis.

In Fig. 3 the profiles of the covariant velocity component $V_3/\sqrt{g_{33}}$ are presented in eight radial sections $\xi^2 = 0$, $0 \le \xi^1 \le 1$; $\xi^2 = \xi^1$, $0 \le \xi^1 \le \sqrt{2}/2$; $\xi^1 = 0$, $0 \le \xi^2 \le 1$; $\xi^2 = -\xi^1$, $-\sqrt{2}/2 \le \xi^1 \le 0$; $\xi^2 = 0$, $-1 \le \xi^1 \le 0$; $\xi^2 = \xi^1$, $-\sqrt{2}/2 \le \xi^1 \le 0$; $\xi^1 = 0$, $-1 \le \xi^2 \le 0$; and $\xi^2 = -\xi^1$, $0 \le \xi^1 \le \sqrt{2}/2$. The calculations showed that at $S/d = 1.5$ the distributions of the contravariant $V^3/\sqrt{g^{33}}$ and covariant $V_3/\sqrt{g_{33}}$ components differ by no more than 2% and the greater this difference the smaller the Reynolds number, which is in qualitative agreement with the earlier obtained results [24, 25].

In Fig. 4 we have plotted the contours of the component $p^*(\xi^1, \xi^2)$ of the dimensionless pressure $p(\xi^1, \xi^2, \xi^3) = C_0\xi^3 + p^*(\xi^1, \xi^2)$. In the case in which $\mathrm{Re} \to 0$ for all R/d the dimensionless pressure contours are horizontally oriented, the pressure increasing from bottom to top. As Re increases (Re = 10 to 80), together with the body force effect, the contours rotate counterclockwise. As a result, the regions with the highest dimensional pressure are located on the outside of the roundness, that is, in the right part of the coil cross-section. The further increase in the Reynolds number (Re = 80 to 1000) causes the formation of local zones with pressure minima in the upper and lower regions of the curved tube.

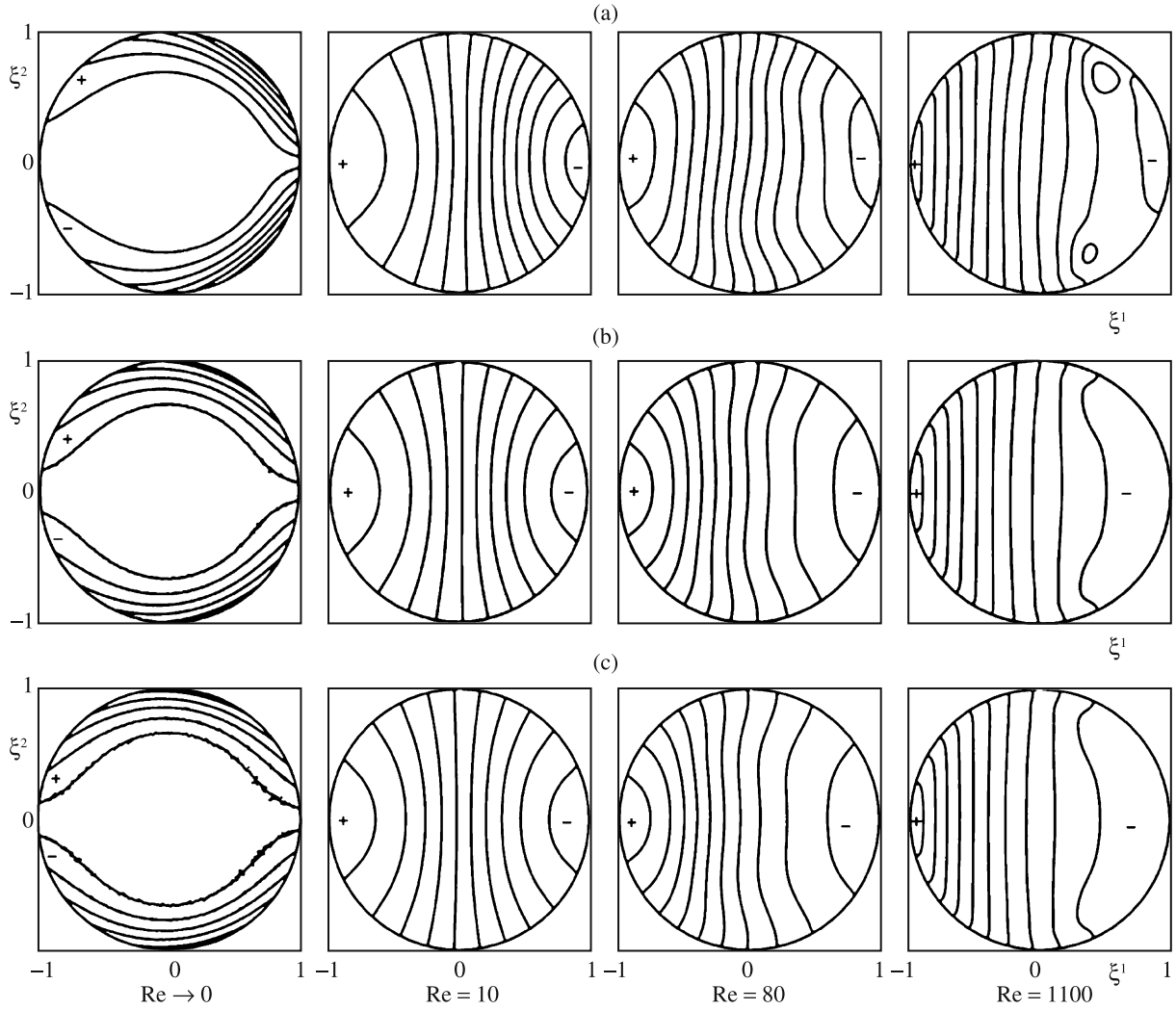

Fig. 4. Contours of the dimensionless pressure p in the cross-section with the relative pitch $S/d = 2.5$ for different Re. Notation same as in Figs. 1 and 2.

The most important for understanding and analyzing the heat transfer in curved coil tubes in an investigation and an assessment of the transverse components of the velocity vector (Figs. 5–7).

In Fig. 5 we have plotted the contours of the horizontal component $V_3/\sqrt{g_{11}}$. Clearly that, as $\mathrm{Re} \to 0$, the channel cross-section can conditionally be subdivided into four regions with different directions of the horizontal velocity component. When $R/d = 1$ or 2.5, the regions on the inner side of the roundness are considerably smaller and pressed against the cross-section boundaries; at grater values of R/d all the four regions are approximately the same. With increase in the Reynolds number the lower right and the upper left regions with the same negative sign of the horizontal velocity component unite into one region. The channel cross-section can be conditionally subdivided into three regions, namely, the upper and lower regions with positive horizontal velocity values and the central region with its negative values. The flow pattern and intensity change with increase in the flow velocity and at $\mathrm{Re} = 1000$ the regions with positive values of the horizontal velocity are pushed toward the outer walls of the coil. The region with negative velocity values enlarges, while the region outline becomes smeared.

As follows from Fig. 6, the vertical velocity components $V_2/\sqrt{g_{22}}$ take positive values, as $\mathrm{Re} \to 0$. As the flow intensity in the upper right and lower left regions of the tube cross-section increases, zones with negative values of the vertical velocity component are formed. Then they develop and at $\mathrm{Re} = 80$ to 100 become comparable with the regions of positive values. With further increase in Re the zones with negative

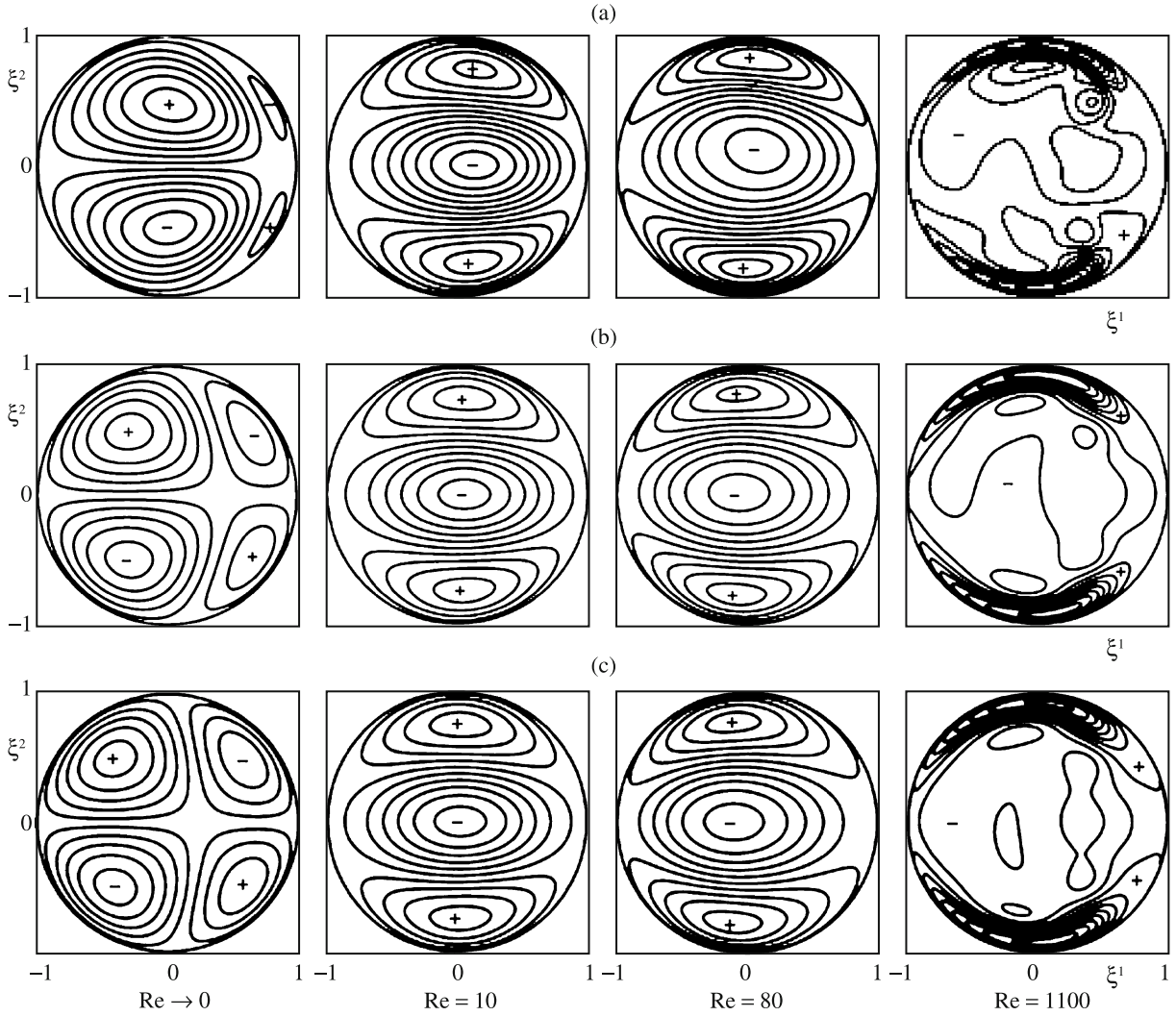

Fig. 5. Contours of the dimensionless horizontal component $V_1/\sqrt{g_{11}}$ of the velocity vector in the cross-section (covariant component) with the relative pitch $S/d = 2.5$ for different Re. Notation same as in Figs. 1 and 2.

and positive values of the vertical velocity component are pushed toward the boundaries of the channel cross-section and new zones are formed in the central region of the channel.

We will present the following general tendency: at small values of R/d the transverse velocity components become comparable with the axial component of the flow velocity directed along the helix and the higher Re the greater their values (Fig. 7). With increase in the coil parameter R/d the transverse velocity components considerably diminish and at $R/d > 10$ they are negligibly small compared with the axial component directed along the helical line. In this case, the coil flow pattern is almost indistinguishable from flows in cylindrical channels with the corresponding cross-sections. At low Reynolds numbers the distributions of the velocity components V_1 and V_2 in the channel cross-section are symmetric. As Re increases, the effect of the inertia factor on the flow pattern becomes increasingly greater and the distributions of the transverse velocity components become asymmetric.

We note that the novelty of the results obtained consists in the fact that the profiles of the velocity components along the lines passing through the center of the cross-section are calculated for the first time. From an analysis of the profiles it follows that at the center of the cross-section the velocity components of the secondary flows can be considerable amounting to one third of the mean-flow-rate velocity. In [32–34], where the orders of the secondary flow velocities are not estimated, the velocity vector fields, or the stream function distributions, in the cross-section are presented, which are the indirect quantitative representations

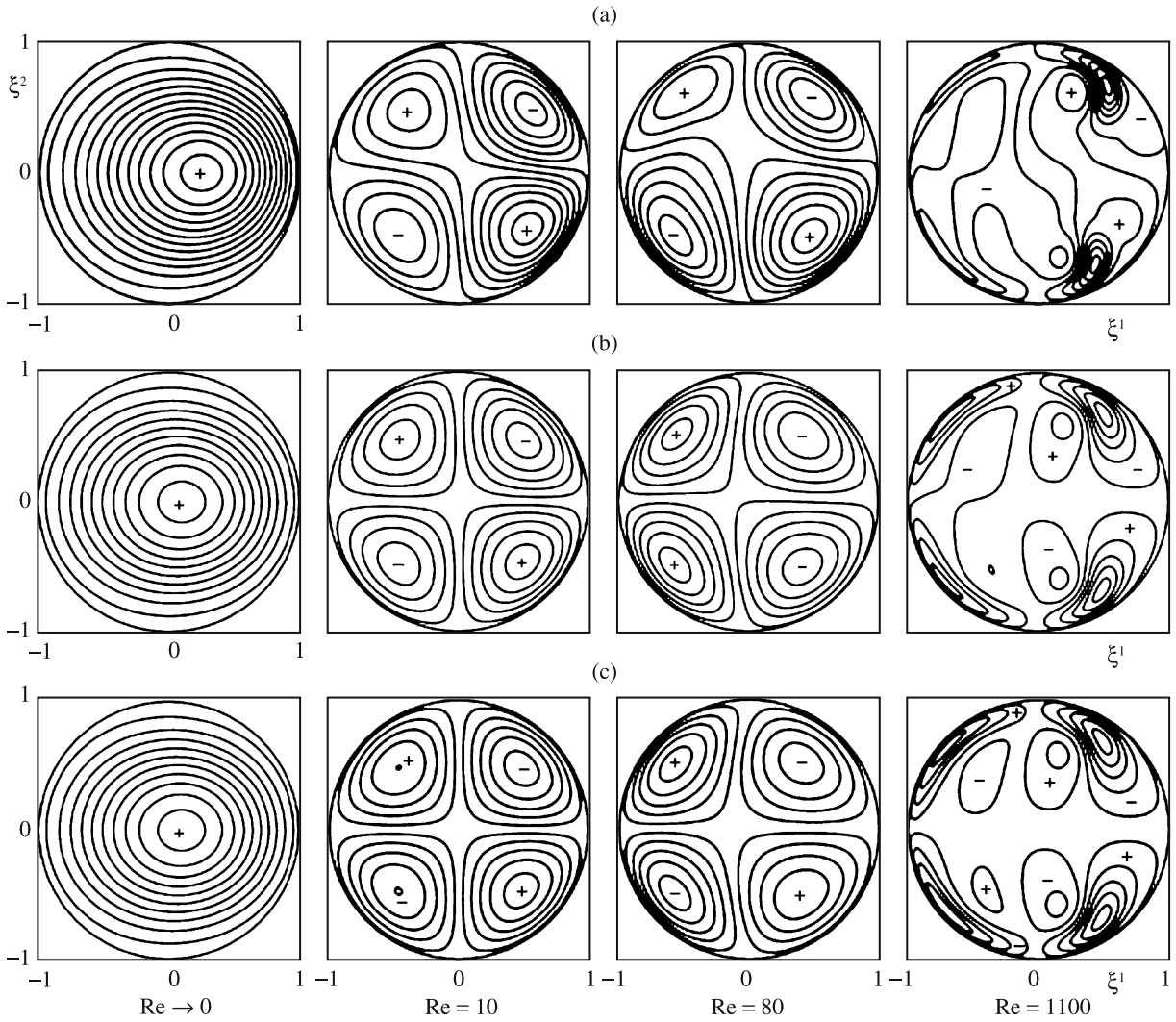

Fig. 6. Contours of the dimensionless vertical component $V_2/\sqrt{g_{22}}$ of the velocity vector in the cross-section (covariant component) with the relative pitch $S/d = 2.5$ for different Re. Notation same as in Figs. 1 and 2.

of the velocity field. Precisely to remove these shortcomings we introduced the new helical coordinate system which is free of singularities at the center of the cross-section. Thus, it makes it possible to obtain the velocity and pressure fields in the cases in which these distributions are asymmetric about the line passing through the vector of the principal normal to the central helical line. On the basis of the calculations performed it can be concluded that at small Reynolds numbers the fields of the secondary flows in the cross-section can be considered as approximately symmetric, so that the orthogonal coordinate system can be used in the calculations [24, 25].

In this study, the helical coordinate system is used, in which in the channel cross-section the natural axes coincide in their directions with the vectors of the principal normal and the binormal. In this case, translation along one of the variables corresponds to the translation along the helical line. This allows one to reduce the solution of the three-dimensional problem to the two-dimensional one without passing to some other variables, to considerably simplify its numerical realization, to obtain particular solutions, and to fairly accurately and fully assess the singularities of the velocity fields in coil tubes for a wide class of channels with similar geometry.

Moreover, the results obtained open the possibility of subsequent wide theoretical investigations and the development of small-scale innovation heat-exchange equipment [1–4] and improved methods of their calculations.

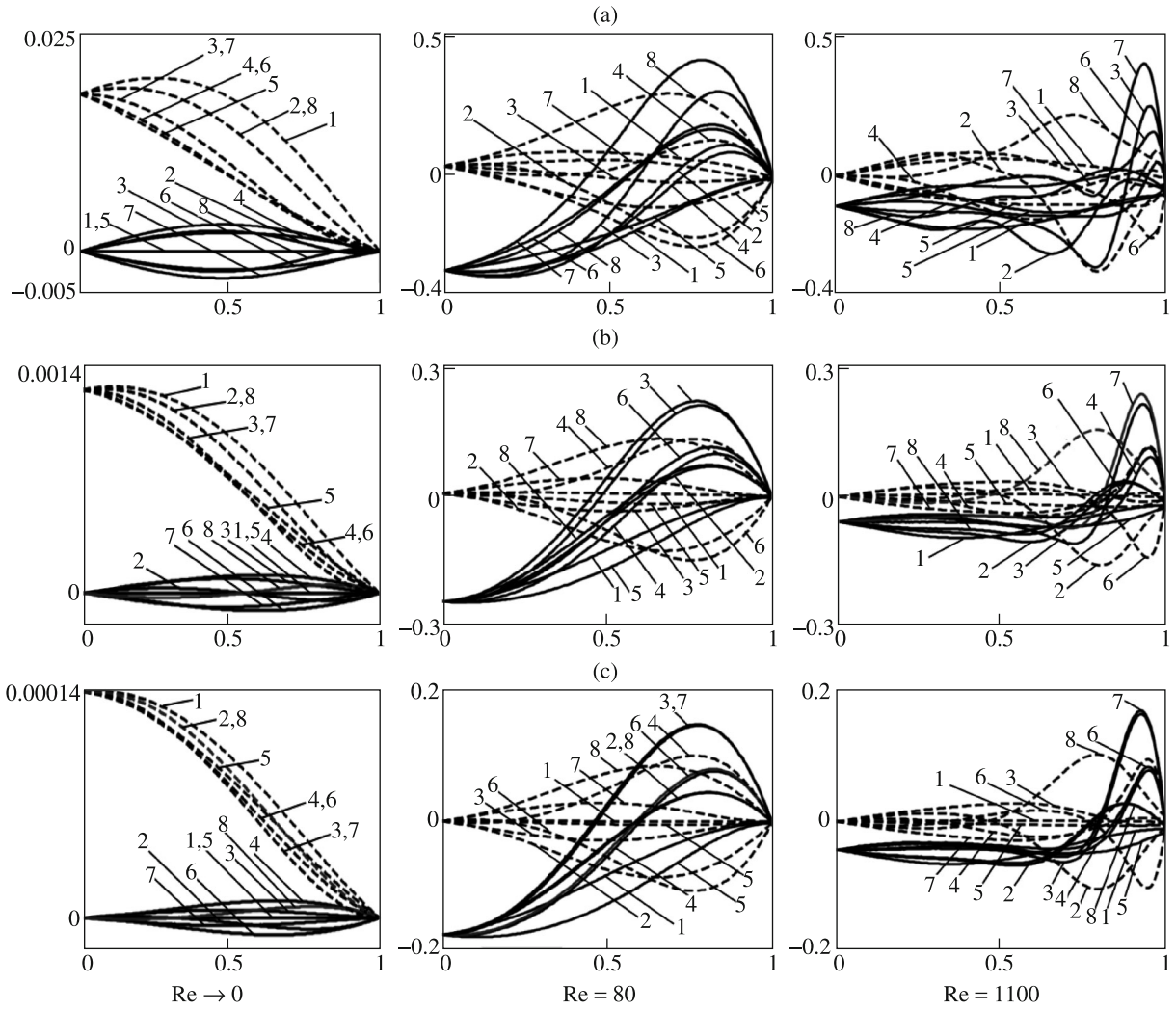

Fig. 7. Profiles of the covariant components of the velocity vector $V_1/\sqrt{g_{11}}$ (broken curves) and $V_2/\sqrt{g_{22}}$ (chain curves) with the relative pitch $S/d = 2.5$ along different lines for different Re. Notation same as in Fig. 3.

Summary. The problem of viscous flow in coil tubes is numerically investigated. The distributions of the axial and transverse velocity components in the coil cross-section are obtained for different values of the Reynolds number and the geometric parameters of the coils. The representation of the behavior of the hydrodynamic fields in the central parts of the coil cross-sections is widened. It is established that at high Reynolds numbers and arbitrary curvatures and torsions the secondary flows can be comparable with the axial flow. It is shown that the velocity field of the secondary flows is asymmetric about the direction determined by the vector of the principal normal to the central helical line.

REFERENCES

1. A.G. Bagoutdinova and Ya.D. Zolotonosov, "Coil Heat Exchangers and Their Mathematical Description," Izv. Vuzov. Stroitelstvo No. 7, 44 (2015).
2. A.Ya. Zolotonosov, Ya.D. Zolotonosov, I.A. Knyazeva, and A.G. Bagoutdinova, "Coil Heat Exchanger. Russian Federation Patent No. 133596," Bullet. Izobr. No. 29 (2013).
3. A.Ya. Zolotonosov, Ya.D. Zolotonosov, and I.A. Knyazeva," "Coil Heat Exchanger Element. Russian Federation Patent No. 155676," Bullet. Izobr. No. 29 (2015).
4. A.Ya. Zolotonosov, Ya.D. Zolotonosov, I.A. Knyazeva, A.G. Bagoutdinova, and E.K. Vachagina, "Coil Heat Exchanger. Russian Federation Patent No. 166177," Bullet. Izobr. No. 10 (2016).
5. Yu.F. Gortyshev, *Heat-Hydraulic Efficiency of Promising Methods of Heat Transfer Intensification in the Channels of Heat Exchange Devices* [in Russian], Kazan (2009).

6. A.I. Leont'ev and V.V. Olimpiev, "Thermophysics and Heat Engineering of Promising Heat Transfer Intensifiers. An Overview," Izv. Ross. Akad. Nauk. Energetika. No. 1, 7 (2011).
7. I.Z. Aronov, "Heat Transfer and Hydraulic Drag in Curved Pipes," Candidate Dissertation, Kiev (1950).
8. V.G. Fastovskii and A.E. Rovinskii, "Investigation of Heat Transfer in a Helical Channel," Teploenergetika No. 1, 39 (1957).
9. V.K. Shchukin, "Generalization of the Experimental Data on Heat Transfer in Coils," Teploenergetika No. 2, 50 (1969).
10. V.K. Shchukin, "Additional Conditions of the Flow Similarity in the Field of Body Inertial Forces," Tr. KAI No. 76, 26 (1963).
11. E.V. Sukhov, "Development of the Structures and the Methods of Calculation of Size-Saving Helical Coil Cooling Elements of Compressor Equipment," Candidate Dissertation, Omsk (2012).
12. P. Gavade Pravin and P.R. Kulkarni, "Experimental Evaluation of Helical Coil Tube in Tube Heat Exchanger," Int. J. Emerging Engineering Research Techn. **3** (2), 12 (2015).
13. V.P. Desial and S.L. Borse, "Experimental Study on Enhancement of Thermal Performance of Wire Wound Tube in Tube Helical Coil Heat Exchanger," IJERA **3**, 340 (2013).
14. Vinodkumar Kiran Voonna and T.K. Tharakeshwar, "Improvement of Heat Transfer Coefficients in a Shell and Helical Tube Heat Exchanger Using Water/Al_2O_3 Nanofluid," IRJET **2**, 213 (2015).
15. Y. Ma, Z. Zhou, J. Wang, Y. Liu, and J. Liang, "Design Optimization of Tube-in-Tube Helical Heat Exchanger Used in JT Refrigerator," in: *Int. Cryocooler Conf. Inc. 09–12 June 2014*, Syracuse Univ., New York (2014).
16. E.A. Krasnoshchekov and A.S. Sukomel, *Handbook on Heat Transfer* [in Russian], Energetika, Moscow (1980).
17. M.N. Manish, G.K. Deshmukh, R.A. Patel, and R.H. Bhoi, "Parametric Analysis of Tube in Tube Helical Coil Exchanger at Constant Wall Temperature," IJSTE **1** (10), 279 (2015).
18. N.M. Triloki, "Modeling and CFD Analysis of Tube in Tube Helical Coil Exchanger," IJSR **4**, 1536 (2015).
19. P. Deshmukh, V.D. Patil, and B. Devakant, "CFD Analysis of Heat Transfer in Helical Coil Tube Heat Exchanger," IJIERT **3** (1), 1 (2016).
20. W.R. Dean and J.M. Hurst, "Note on the Motion of Fluid in a Curved Pipe," Phil. Mag. **20** (4), 208 (1927).
21. W.R. Dean and J.M. Hurst, "The Streamline Motion of Fluid in a Curved Pipe," Phil. Mag. **5** (30), 673 (1928).
22. H.G. Cuming, "The Secondary Flow in Curved Pipes," Aeronautical Res. Council. Report No. 2880 (1952).
23. D.J. Mcconaloguanen and D.R. Srivastava, "Motion of a Fluid in a Curved Tube," Proc. Roy. Soc. London. Ser. A **307**, 37 (1968).
24. M. Germano, "On the Effect of Torsion on a Helical Pipe Flow," J. Fluid Mech. **125**, 1 (1982).
25. M. Germano, "The Dean Equations Extended to a Helical Pipe Flow," J. Fluid Mech. **203**, 289 (1989).
26. T.J. Hüttl, "Navier–Stokes Solutions of Laminar Flows Based on Orthogonal Helical Coordinates," Numer. Methods in Laminar and Turbulent Flow **10**, 191 (1997).
27. M. Vasudevaian and R. Rajalakshmi, "Flow in a Helical Pipe," J. Appl. Math. **19**, 75 (1988).
28. M. Vasudevaian and R. Patturaj, "Effect of Torsion in a Helical Pipe Flow," Int. J. Math. Math. Sci. **17**, 553 (1994).
29. D.G. Dritschel, "Generalized Helical Beltrami Flows in Hydrodynamics and Magnetohydrodynamics," J. Fluid Mech. **222**, 525 (1991).
30. Lei Xue, "Study on Laminar Flow in Helical Circular Pipes with Galerkin Method," Computers Fluids **31**, 113 (2002).
31. Z. Zapryanov, Ch. Christov, and E. Toshev, "Fully Developed Laminar Flow and Heat Transfer in Curved Tubes," Int. J. Heat Mass Transfer **23**, 873 (1980).
32. L.C. Truesdell, R.J. Adler, "Numerical Treatment of Fully Developed Laminar Flow in Helically Coiled Tubes," A.I. Ch.E.J. **16**, 1010 (1970).
33. S.V. Patankar, V.S. Pratap, and D.B. Spalding, "Prediction of Laminar Flow and Heat Transfer in Helically Coiled Pipes," J. Fluid Mech. **62**, 539 (1974).
34. A.N. Dravid, K.A. Smith, E.W. Merrill, and P.L.T. Brian, "Effect of Secondary Fluid Motion on Laminar Flow Heat Transfer in Helically Coiled Circular Pipes," AIChEJ **17**, 1114 (9171).
35. Yu.G. Namzeev, *Fluid Dynamics and Heat Transfer of Swirled Flows of Rheologically Complex Media* [in Russian], Energoizdat, Moscow (1996).